https://doi.org/10.5194/egusphere-2026-1786
Preprint. Discussion started: 30 April 2026

Photochemical mechanism–dependent ozone formation and precursor sensitivity under varying NO_x conditions

Yuelin Liu[1,2†], Yuanjun Gong[3†], Nan Wang[2*], Guangming Shi[1,2], Fumo Yang[1,2], Yuanhang Zhang[3], Keding Lu[3*]

[1]College of Architecture & Environment, Sichuan University, Chengdu, 610207, China

[2]College of Carbon Neutrality Future Technology, Sichuan University, Chengdu, 610207, China

[3]College of Environmental Sciences and Engineering, Peking University, Beijing, 100871, China

Correspondence to: Keding Lu (k.lu@pku.edu.cn); Nan Wang (nan.wang@scu.edu.cn)

Yuelin Liu and Yuanjun Gong have the same contribution to this work.

https://doi.org/10.5194/egusphere-2026-1786
Preprint. Discussion started: 30 April 2026

Abstract. Photochemical mechanisms are core components of air quality models, yet differences among them introduce substantial uncertainty in ozone (O_3) simulations. Here, we systematically evaluate three widely used mechanisms (CB06, SAPRC07, and RACM2) using the CMAQ model during an O_3 pollution episode in Chengdu, China. To ensure consistency, a customized volatile organic compounds emission inventory was developed for RACM2. The results show pronounced inter-mechanistic differences in simulated O_3, radical chemistry, and precursor sensitivities under distinct NO_x conditions. SAPRC07 and RACM2 produced higher and comparable O_3 levels (~95 ppbv) with better performance in urban areas, whereas CB06 simulated lower O_3 (~80 ppbv) and performed better under low-NO_x conditions. These differences are linked to variations in radical concentrations and reaction pathways, with RACM2 yielding the highest OH levels, SAPRC07 better capturing HO_2, and CB06 simulating lower RO_2. Despite these discrepancies, all mechanisms consistently reproduced the dominant O_3 formation pathway, with RO_2 + NO contributing over 50% of net production. However, radical sources and termination pathways differed substantially between urban and suburban environments, reflecting regime-dependent chemistry. Sensitivity analysis further shows that anthropogenic aromatics and alkenes dominate urban O_3 formation, whereas biogenic emissions dominate in suburban areas. Notably, O_3 sensitivity to biogenic emissions is higher in urban high-NO_x conditions, highlighting an amplified biogenic contribution. These findings demonstrate that mechanism choice fundamentally affects O_3 formation and precursor sensitivities, emphasizing the need for multi-mechanism approaches to improve model reliability and support effective emission control strategies.

https://doi.org/10.5194/egusphere-2026-1786
Preprint. Discussion started: 30 April 2026

1 Introduction

Ozone (O_3) is a potent oxidant in the atmosphere, playing a key role in the oxidation of trace gases in the troposphere and regulating their atmospheric lifetimes. However, the high concentrations of surface O_3 represent a significant environmental and public health challenge, as they are known to cause serious harm to human health and vegetation (Ashmore, 2005; Li et al., 2025b). Tropospheric O_3 is also a significant greenhouse gas via radiative effect (Kuai et al., 2017; Li et al., 2018). Due to its impacts on air quality and climate change, O_3 has remained a focus of sustained attention from the scientific communities and governments over the past decades. As the highly non-linear relationship between O_3 and its precursors (i.e., NO_x and volatile organic compounds (VOC)), the significant reduction of primary pollutants even increased O_3 concentrations in China and the concentration of O_3 have remained persistently high (Fu et al., 2020; Han et al., 2024; Huang et al., 2021; Liu and Wang, 2020; Nelson et al., 2024; Yan et al., 2024).

O_3 in the atmosphere is formed by the combination of oxygen atoms ($O(^3P)$) and oxygen molecules (O_2) (shown as Reaction R1). $O(^3P)$ is primarily generated via the photolysis of NO_2 at wavelengths $\lambda \leq 424$ nm (R2). In theory, once O_3 formed, it readily reacts with NO to regenerate NO_2 (R3). That is, in the absence of other chemical species, reactions ((e.g., R1-R3) will form a closed loop and result in no net O_3 accumulation. However, in the real atmosphere, other key oxidizing agents such as hydroperoxyl radical (HO_2) and organic peroxyl radical (RO_2) radicals in the troposphere can also oxidize NO to NO_2 (e.g., R4–R5). These reactions compete with R3, reducing the consumption of O_3 through reaction with NO and thus leading to O_3 accumulation (Wang et al., 2017). Under the action of the "NO_x cycle" formed by R2, R4, and R5, O_3 is efficiently generated without the consumption of NO_x.

$$O(^3P) + O_2 + M \rightarrow O_3 + M \quad \text{(R1)}$$

$$NO_2 + h\nu \rightarrow O(^3P) + M \quad \text{(R2)}$$

$$O_3 + NO \rightarrow NO_2 + O_2 \quad \text{(R3)}$$

$$HO_2 + NO \rightarrow NO_2 + OH \quad \text{(R4)}$$

$$RO_2 + NO \rightarrow NO_2 + RO \quad \text{(R5)}$$

In addition to "NO_x cycle", O_3 formation is also affected by the RO_x (RO_x = OH + HO_2 + RO_2) radical cycle. The RO_x radicals cycle continuously generates HO_2 and RO_2 radicals, promoting the oxidation of

https://doi.org/10.5194/egusphere-2026-1786
Preprint. Discussion started: 30 April 2026

NO to NO_2 by HO_2 and RO_2 and facilitating O_3 formation. The primary RO_x radicals play a crucial role in driving the RO_x cycle. The sources of primary RO_x radicals mainly include the photolysis of O_3, nitrous acid (HONO), formaldehyde (HCHO), and other carbonyls, and the ozonolysis reaction of O_3 with alkenes (Zhou et al., 2024; Yang et al., 2021; Xue et al., 2016; Wang et al., 2017). The importance of individual sources may vary considerably from one region to another. For instance, hydroxyl radical (OH) radicals are mainly produced by O_3 photolysis at wavelengths below 320 nm (R6–R7) in the troposphere (Hofzumahaus et al., 1992), whereas in polluted urban areas, HONO photolysis becomes its dominant primary source (R8) (Tan et al., 2017; Tan et al., 2026). In addition, the RO_x radical cycle is typically initiated by the reaction of the OH radical with VOC, generating RO_2 radicals (R9). Then it proceeds via reaction R9 to form RO radicals and produce HO_2 radicals and carbonyl compounds (R11). Subsequently, HO_2 reacts with NO as shown in Reaction 4, regenerating OH radicals and oxidizing NO to NO_2. Therefore, each complete RO_x cycle converts two molecules of NO into NO_2, resulting in the net production of two molecules of O_3.

$$O_3 + h\nu \rightarrow O(^1D) + O_2 \quad \text{(R6)}$$

$$O(^1D) + H_2O \rightarrow OH + OH \quad \text{(R7)}$$

$$HONO + h\nu \rightarrow OH + NO \quad \text{(R8)}$$

$$VOCs + OH \rightarrow RO_2 + H_2O \quad \text{(R9)}$$

$$RO_2 + NO \rightarrow NO_2 + RO \quad \text{(R10)}$$

$$RO + O_2 \rightarrow HO_2 + carbonyls \quad \text{(R11)}$$

The "RO_x cycle" and "NO_x cycle" can be terminated through mutual self-reaction among RO_x radicals or via the reactions with NO_x, preventing the explosive of RO_x radicals in the atmosphere. Under high NO_x conditions, the termination of the RO_x and NO_x cycles is primarily dominated by reactions of NO_2 with OH and RO_2 radicals (R12–R13). In contrast, under low NO conditions, the termination of radical chain is mainly driven by the self-reaction of HO_2 radicals and cross-reactions between HO_2 and RO_2 radicals (R14–R15), which further produce hydrogen peroxide (H_2O_2) and organic hydroperoxides (ROOH). Therefore, the ratio of major products or its production rates from termination reactions, such as H_2O_2 to HNO_3, can indicate whether the ambient atmosphere is under high or low NO_x conditions.

https://doi.org/10.5194/egusphere-2026-1786
Preprint. Discussion started: 30 April 2026

This ratio is commonly used as an indicator for determining O_3 formation regimes (Wei et al., 2018; Liu et al., 2010; Cordiner et al., 2002).

$$NO_2 + OH \rightarrow HNO_3 \quad \text{(R12)}$$

$$NO_2 + RO_2 \rightarrow RONO_2 \quad \text{(R13)}$$

$$HO_2 + HO_2 \rightarrow H_2O_2 \quad \text{(R14)}$$

$$HO_2 + RO_2 \rightarrow ROOH + O_2 \quad \text{(R15)}$$

As discussed above, photochemically produced O_3 is a secondary pollutant formed from its precursors through a series of highly nonlinear photochemical reactions (e.g., the RO_x and NO_x cycles). Due to the complexity of atmospheric chemical processes, accurate simulation of O_3 formation remains challenging. Given the limitations of field observations or laboratory simulations in fully representing O_3 regional characteristics, air quality models have become essential tools for quantitatively understanding O_3 formation mechanisms and evaluating emission control strategies. Moreover, the ability of the air quality model to accurately simulate the nonlinear relationships between O_3 and its precursors depends largely on the atmospheric photochemical mechanism it employs. Since the first tropospheric chemical mechanism was proposed in the 1960s (Friedlander and Seinfeld, 1969), extensive research on atmospheric chemical mechanisms has been conducted by scholars worldwide over the past few decades. As far, the atmospheric photochemical mechanisms widely used include the Master Chemical Mechanism (MCM) (Jenkin et al., 2015), Carbon Bond Mechanism (CBM) (Luecken et al., 2019), Statewide Air Pollution Research Center mechanism (SAPRC) (Carter, 1996), and Regional Atmospheric Chemistry Mechanism (RACM) (Goliff et al., 2013), and so on. From the perspective of chemical species, these photochemical mechanisms are generally divided into explicit reaction mechanisms and lumped reaction mechanisms (Dodge, 2000). Explicit reaction mechanism includes all species involved in a chemical reaction, while a lumped reaction mechanism groups together species with similar chemical properties. Given the high computational demands of explicit reaction mechanisms, lumped chemical mechanisms such as CBM, SAPRC and RACM are the mainstream choices for in the air quality model. These schemes utilize two distinct lumping approaches: structural classification (i.e., carbon-bond or functional groups, such as CBM) and reactivity-based classification (such as SAPRC and RACM).

https://doi.org/10.5194/egusphere-2026-1786
Preprint. Discussion started: 30 April 2026

The CBM classified by carbon-bond structures is the most widely applied chemical mechanism in air quality modeling studies for its low computational cost and the relative ease of obtaining emission inventories (Liu et al., 2023). Unlike the CBM, the SAPRC mechanism classifies organic species according to their OH reactivity and features the detailed description of reactions involving specific VOCs (Carter, 1996). However, this level of detail significantly increases computational cost requirement and limit the efficiency of its extensive application. The RACM mechanism is similar to that of the SAPRC mechanism, albeit with different criteria for classification by OH reactivity (Goliff et al., 2013). It preserves the carbon structure of emitted species, explicitly simulates individual peroxyl radicals, and minimizes reliance on lumped species which often referred to as operators for radical cycle. These attributes make RACM2 particularly well-suited for comparison with observational data, ensure transparency in the mapping of emission inventories, and provide flexibility for modification and further expansion. And RACM maintains computational efficiency used in regulatory applications, comparable to SAPRC mechanisms.

In China, the CBM and SAPRC mechanisms have been widely applied in air quality models, whereas RACM is predominantly used in box models (Liu et al., 2023). The limited application of RACM in three-dimensional air quality simulations in China is likely attributable to the difficulty in obtaining compatible emission inventories. Previous study has evaluated the uncertainties associated with four photochemical mechanisms: SAPRC07TC, SAPRC99, CB05TUCL, and RACM2 in simulating O_3 concentrations over Japan. The results indicated that the differences in O_3 concentrations among the chemical mechanisms were within 10 ppb over Japan. Specifically, the O_3 concentrations simulated by CB05TUCL were lower than those produced by SAPRC07TC, whereas the simulation results from RACM2 were comparable to those from SAPRC07TC over inland Japan (Kitayama et al., 2019). Moreover, there was also other study indicating that SAPRC07 outperforms CB06 in predicting peak O_3 during exceedances in the Great Bay Area, for more detailed VOC treatment in SAPRC07 (Li et al., 2025a). In China, a recent comparative study using box models have demonstrated that, relative to RACM2, the CB06 and SAPRC07 mechanisms tend to underestimate OH concentrations, which may subsequently lead to an underestimation of O_3 levels (Liu et al., 2023). However, there are few research about investigate the uncertainty in simulating O_3 pollution over China for three-dimensional air quality model arising from different photochemical mechanisms.

https://doi.org/10.5194/egusphere-2026-1786
Preprint. Discussion started: 30 April 2026

Chengdu, a megacity in southwest China, covers a total area of about 14335 square kilometers, and the resident population was more than 20 million in 2025. In recent years, the total gross domestic product (GPD) of Chengdu was increasing rapidly, around 2.35 trillion dollars in 2024 (available at https://www.sc.gov.cn/, in Chinese). It is designated as one of the important central cities in the western region, and expected to be one of the economic centers in western China. Its features dense urban population, advanced industry and the highest car ownership in China, leading to high intensity of anthropogenic emissions (Wang et al., 2022; Zhou et al., 2019). Affected by the terrain of the unique deep basin and unfavorable meteorological conditions (Shu et al., 2021; Zhang et al., 2019), O_3 and its precursors in Chengdu are prone to accumulate and recycle in the local atmosphere (Wang et al., 2024; Tan et al., 2018). During 2022-2024 year, the 90th percentile of the maximum daily 8-hour average (MDA8) O_3 concentration in Chengdu (https://sthj.chengdu.gov.cn/) was 168 ~ 181 μg/m^3, continuously exceeding the secondary standard of the Ambient Air Quality Standard (GB3095-2012). Therefore, sustained investigation into the photochemical formation mechanisms and mitigation frameworks for O_3 pollution in Chengdu is imperative. A more profound understanding and mechanistic discrepancies under varying NOx conditions within this region is essential for refining model evaluation and enhancing the reliability of predictive simulations.

To evaluate the chemical mechanism uncertainty under varying NO_x conditions, the O_3 episode in Chengdu from August 9 to 18, 2019 were simulated using the Community Multiscale Air Quality (CMAQ) model (Byun and Schere, 2006) with three chemical mechanisms (CB06, RACM2 and SAPRC07). And we constructed a VOC emission inventory for the RACM2 mechanism through species mapping method. Then the difference among the three mechanisms of concentrations of simulated O_3 and key photochemical pollutants, O_3 budget, RO_x cycle and the sensitivity of O_3 to its precursor emission under high-NO_x urban condition and low-NO_x condition were discussed. This study helps to profoundly understand the difference among different photochemical mechanisms and identify the key driver of O_3 formation under varying NO_x condition, and benefits the mechanism selection for provide scientific and the formulation of precise emission control strategies.

https://doi.org/10.5194/egusphere-2026-1786
Preprint. Discussion started: 30 April 2026

2 Data and methods

2.1 Site descriptions and observational data

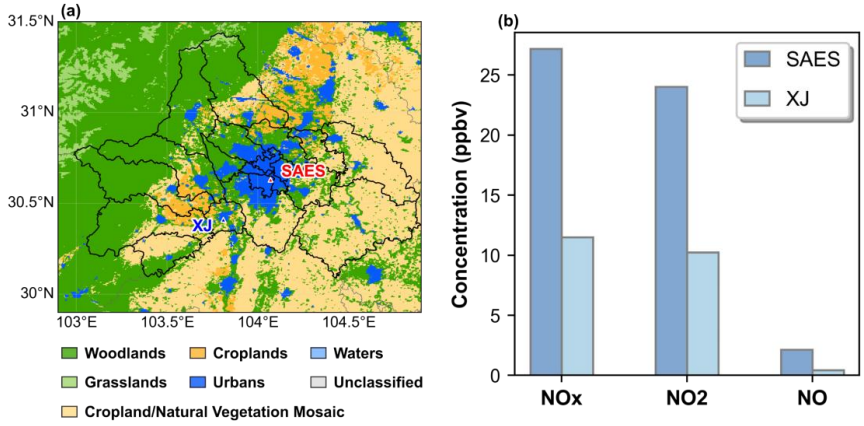

Figure 1 (a) Land use types in Chengdu and surrounding areas, along with the locations of the SAES site (red triangle) and XJ site (blue triangle). (b) Mean concentrations of NO_x (NO_x = NO +NO_2), NO_2 and NO at the Sichuan Academy of Environmental Sciences (SAES) site and Xinjin (XJ) site during this pollution episode.

Located in southwestern China, Chengdu features a heterogeneous landscape that transitions from dense urban environments to peripheral croplands and woodlands (Fig. 1a). To investigate mechanistic discrepancies under varying NO_x conditions, we conducted in-situ field observations at two contrasting sites during an O_3 pollution episode from August 9 to 18, 2019. The Sichuan Academy of Environmental Sciences (SAES) site, situated in urban core, represents a typical high-NO_x environment. Conversely, the Xinjin (XJ) site, characterized by more extensive vegetation cover, serves as a representative low-NO_x suburban environment. During this O_3 episode, the concentrations of NO_x at SAES were significantly higher than those at XJ (Fig. 1b), reflecting a sharp urban-suburban emission gradient. We obtained hourly concentration data for key photochemical species, including O_3, NO_x, HONO, isoprene (ISOP), and HNO_3 at the urban site (SAES), and O_3, NO_x, HONO, ISOP, and formaldehyde (HCHO) at the suburban site (XJ). Furthermore, hourly concentrations of atmospheric radicals (OH and HO_2) were measured at the XJ site using the Peking University laser-induced fluorescence system (PKU-LIF). This system, which utilizes the fluorescence assay by gas expansion (FAGE) technique, has been widely

https://doi.org/10.5194/egusphere-2026-1786
Preprint. Discussion started: 30 April 2026

applied in field campaigns across China to provide high-fidelity radical measurements (Lu et al., 2012; Ma et al., 2019; Tan et al., 2017).

Besides, network monitoring hourly O_3 and NO_2 data were also obtained from the China National Environmental Monitoring Center (https://air.cnemc.cn:18007/). Detail location information of the monitoring sites are as shown in the Table S1.

2.2 WRF-CMAQ Modeling

The CMAQ (version 5.5) simulations were performed using two-way nested domains, consisting of a 27 km outer domain covering China and a 3 km inner domain focused on the Chengdu Plain (Fig. S1). Three photochemical mechanisms were evaluated using their respective gas-phase and aerosol modules: cb6r5_ae7_aq (Luecken et al., 2019), saprc07tic_ae7i_aq (Xie et al., 2013) and racm2_ae6_aq (Sarwar et al., 2013), representing the CB06, SAPRC07, and RACM2 photochemical mechanisms, respectively. Meteorological forcing was provided by the Weather Research & Forecasting Model (WRF) version 4.6, with specific physics configurations detailed in Table S2. Biogenic emissions were prepared using the Model of Emissions of Gases and Aerosols from Nature (MEGAN) version 3.2 (Guenther et al., 2012), while anthropogenic emissions were derived from the Multi-resolution Emission Inventory for China (MEIC) (Zheng et al., 2018; Li et al., 2017; Geng et al., 2024). To address discrepancies in VOC species across mechanisms, different mapping strategies were employed. While VOC emissions for SAPRC07 are provided directly by the MEIC inventory, those for CB06 were derived via mapping from the CB05 and SAPRC07 schemes following the methodology described in Huang et al. (2023). To ensure inter-mechanistic consistency, a customized VOC emission inventory for RACM2 was specifically constructed through species mapping based on the MEIC database (see Section 2.3 and Table 1 for details). A summary of the VOC inputs for all three mechanisms is provided in Table S3. For each simulation, a 3-day spin-up period was utilized to minimize the influence of initial conditions.

To quantify the reaction rates of individual chemical reaction or combinations of chemical reaction, the Integrated Reaction Rate (IRR) analysis module of CMAQ was employed. This diagnostic tool allows for a detailed assessment of the influence of specific chemical pathways on O_3 concentrations. Moreover, to identify key primary precursor emission driving O_3 formation, the Decoupled Direct Method in Three Dimensions (DDM) module was used to calculate the sensitivities of O_3 to NO_x and primary VOC emission. CMAQ DDM can directly calculate the first-order sensitivity of pollutant concentrations to

https://doi.org/10.5194/egusphere-2026-1786
Preprint. Discussion started: 30 April 2026

emission changes, eliminating the need for re-simulations and greatly reducing computational costs and simulation uncertainties (Dunker, 1984; Dunker et al., 2002).

2.3 Development of a customized emission inventory for RACM2

To evaluate the performance of the RACM2 mechanism in simulation atmospheric photochemical pollution, we developed a customized VOC emission inventory. This was necessitated by the fact that the mainstream MEIC database does not directly provide anthropogenic VOC emissions tailored for RACM2. Consequently, we constructed this inventory through species mapping, leveraging existing MEIC data for other chemical mechanisms including CB05, SAPRC99, SAPRC07, and RADM2. The detailed mapping protocols are summarized in Table 1. Notably, the conversion of RADM2_XYL to RACM2_XYM, RACM2_XYP, and RACM2_XYO was informed by sector-specific proportions of these species in established VOC emission profiles (Sha et al., 2021).

Table 1 The mapping between VOC emissions of RACM2 mechanism and other chemical mechanism in the MEIC inventory

RACM2 Species	MEIC Inventory Species	Factor	Description
ACD	SAPRC99_CCHO	1	Acetaldehyde
ACE	SAPRC07_ACYE	1	Acetylene
ACT	SAPRC07_ACET	1	Acetone
ALD	SAPRC99_RCHO	1	C3 and higher aldehydes
API	CB05_TERP	1	Alpha-pinenes and other cyclic terpenes with one double bond
BALD	SAPRC07_BALD	1	Benzaldehyde and other aromatic aldehydes
BEN	SAPRC07_BENZ	1	Benzene
CH4	RADM2_CH4	1	Methane
CSL	SAPRC99_CRES	1	Cresol and other hydroxy substituted aromatics
EOH	CB05_ETOH	1	Ethanol
ETE	RADM2_OL2	1	Ethene
ETH	RADM2_ETH	1	Ethane
GLY	RADM2_GLY	1	Glyoxal
HC3	RADM2_HC3	1	Alkanes, esters and alkynes with HO rate constant (298 K, 1 atm) less than 3.4×10-12
HC3	SAPRC07_ACYE	-1	Alkanes, esters and alkynes with HO rate constant (298 K, 1 atm) less than 3.4×10-12

https://doi.org/10.5194/egusphere-2026-1786
Preprint. Discussion started: 30 April 2026

HC5	RADM2_HC5	1	Alkanes, esters and alkynes with HO rate constant (298 K, 1 atm) between 3.4×10 -13 and 6.8×10-12
HC8	RADM2_HC8	1	Alkanes, esters and alkynes with HO rate constant (298 K, 1 atm) greater than 6.8×10-12
HCHO	RADM2_HCHO	1	Formaldehyde
ISO	RADM2_ISO	1	Isoprene
KET	RADM2_KET	1	Ketones
MACR	SAPRC07_MACR	1	Methacrolein
MEK	SAPRC07_MEK	1	Methyl ethyl ketone
MGLY	RADM2_MGLY	1	Methylglyoxal and other alpha-carbonyl aldehydes
MOH	SAPRC07_MEOH	1	Methanol
MVK	RADM2_MVK	1	Methyl vinyl ketone
OLI	RADM2_OLI	1	Internal alkenes
OLT	RADM2_OLT	1	Terminal alkenes
ORA1	RADM2_ORA1	1	Formic acid
ORA2	RADM2_ORA2	1	Acetic acid and higher acids
PHEN	SAPRC99_PHEN	1	Phenol
TOL	RADM2_TOL	1	Toluene and less reactive aromatics
UALD	SAPRC07_IPRD	1	Unsaturated aldehydes
XYM	RADM2_XYL	/	M-xylene
XYP	RADM2_XYL	/	P-xylene
XYO	RADM2_XYL	/	O-xylene

2.4 Analytical framework for O_3 formation budget

In the troposphere, the oxidation of NO to NO_2 by HO_2 and RO_2 radicals drives the gross production of O_3. Following this mechanism, the gross O_3 formation rate ($F(O_3)$) is calculated using Equation (1), where k represents the bimolecular reaction rate constant. Conversely, O_3 loss pathways include O_3 photolysis and reactions with alkenes, OH radicals, and HO_2 radicals. Additionally, the reaction of NO_2 with OH radicals, which effectively removes NO_x from the cycle by forming HNO_3, is also accounted for one of the O_3 loss pathways. The total O_3 destruction rate ($D(O_3)$) is determined via Equation (2). Consequently, the net O_3 production rate $P(O_3)$ is defined as the difference between the gross O_3 formation rate and the O_3 destruction rate, as shown in Equation (3).

$$F(O_3) = k_{[HO_2,NO]}[HO_2][NO] + k_{[RO_2,NO]}[RO_2][NO] \quad (1)$$

https://doi.org/10.5194/egusphere-2026-1786
Preprint. Discussion started: 30 April 2026

$$D(O_3) = k_{[O^1D,H_2O]}[O^1D][H_2O] + k_{[O_3,Alkenes]}[Alkenes][NO] + k_{[O_3,OH]}[O_3][OH] +\backslash$$

$$k_{[O_3,HO_2]}[O_3][HO_2] + k_{[NO_2,OH]}[NO_2][OH] \quad (2)$$

$$P(O_3) = F(O_3) - D(O_3) \quad (3)$$

3 Results and discussion

3.1 Inter-mechanistic evaluation of modeled O_3 and key precursors

3.1.1 Evaluation of inter-mechanistic O_3 simulation

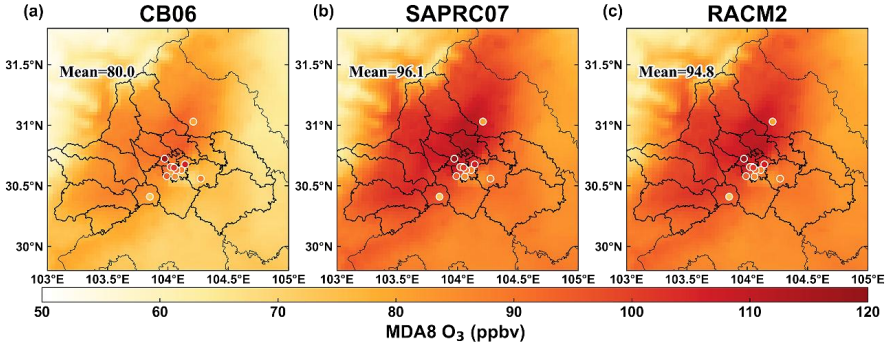

Figure 2 Regional distribution of maximum daily 8-hour average (MDA8) O_3 concentration simulated by three photochemical mechanisms (CB06, SAPRC07 and RACM2) during August 9-August 18, 2019. The solid dots represent the site-observed mean MDA8 O_3 concentrations.

Fig. 2 illustrates the spatial distribution of MDA8 O_3 concentrations simulated by the CB06, SAPRC07, and RACM2 mechanisms during the O_3 pollution episode (9–19 August 2019). In general, the CB06 mechanism simulated the lowest O_3 concentrations, while the SAPRC07 and RACM2 mechanisms simulated higher, comparable levels with largely consistent spatial patterns. Specifically, the regional mean MDA8 O_3 for SAPRC07 and RACM2 in the Chengdu area were 96.1 ppbv and 94.8 ppbv, respectively, exceeding the 80.0 ppbv simulated by CB06. The corresponding biases for SAPRC07 and RACM2 were -16.1 ppbv and -14.8 ppbv, respectively. Compared with monitoring station observations, the MDA8 O_3 concentrations simulated by SAPRC07 and RACM2 in the Chengdu urban area were in better agreement with the observations, while those simulated by CB06 were significantly lower. In contrast, at suburban sites such as XJ, SAPRC07 and RACM2 tended to overestimate MDA8 O_3 concentrations relative to observations, whereas the CB06 simulations were more consistent with the observed values.

https://doi.org/10.5194/egusphere-2026-1786
Preprint. Discussion started: 30 April 2026

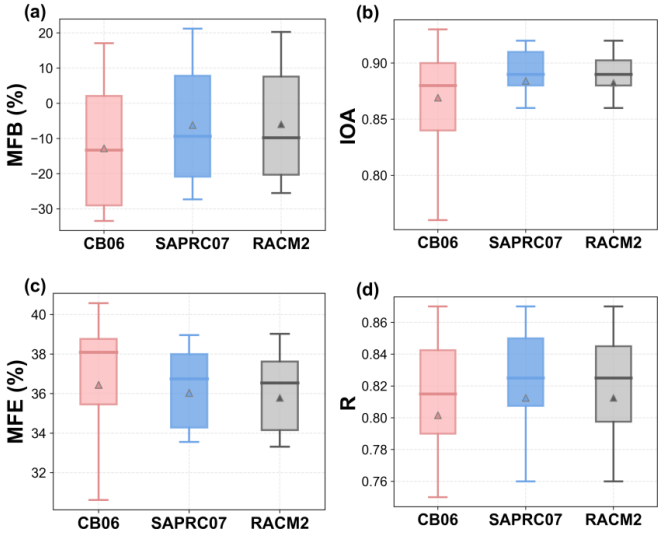

Figure 3 Statistical analysis of hourly O_3 simulated by three photochemical mechanisms (CB06, SAPRC07 and RACM2) across Chengdu region during August 9-August 18, 2019. The box plots present the 10th, 25th, 50th, 75th, and 90th percentiles of the statistical metrics individually. The triangle in the box plot denotes the mean value.

To validate the performance of three photochemical mechanisms in simulating O_3 pollution, we adopted statistical metrics to evaluate the discrepancies between simulated results and observed values (Fig. 3). The specific calculation methods for the statistical metrics are presented in Table S4. In general, SAPRC07 and RACM2 exhibited comparable simulation performance for hourly O_3 concentrations, whereas the CB06 mechanism showed slightly lower performance and a marked underestimation of O_3 levels. Statistical evaluation indicates that all three mechanisms met the established benchmarks for model performance (MFB < ±35%, MFE < 65%, R > 0.6, and IOA > 0.7) (Huang et al., 2025). In specific, SAPRC07 and RACM2 exhibited the most robust and comparable performance, yielding identical median correlation coefficients (R = 0.83) and Index of Agreement (IOA = 0.89). While still within acceptable limits, CB06 showed a more pronounced underestimation of O_3 levels, with a median MFB of -13.63% and slightly higher error metrics (MFE = 38.15%) compared to the other two schemes. Previous study has attributed the underestimation of O_3 by CB06 to its insufficient consideration of the NO_2 recycling pathway from nitrates, leading to lower simulated NO_2 concentrations and consequently reduced O_3 formation (Luecken et al., 2019). Although the O_3 simulation performance of CB06 is inferior to that of SAPRC07 and RACM2, the evaluation of photochemical mechanisms cannot be adequately

https://doi.org/10.5194/egusphere-2026-1786
Preprint. Discussion started: 30 April 2026

assessed based solely on O_3 simulation performance. To comprehensively evaluate the performance of the three photochemical mechanisms in simulating O_3 pollution, further in-depth comparative analysis with other indicators is essential.

3.1.2 Discrepancies in key photochemical intermediates under distinct NO_x environments

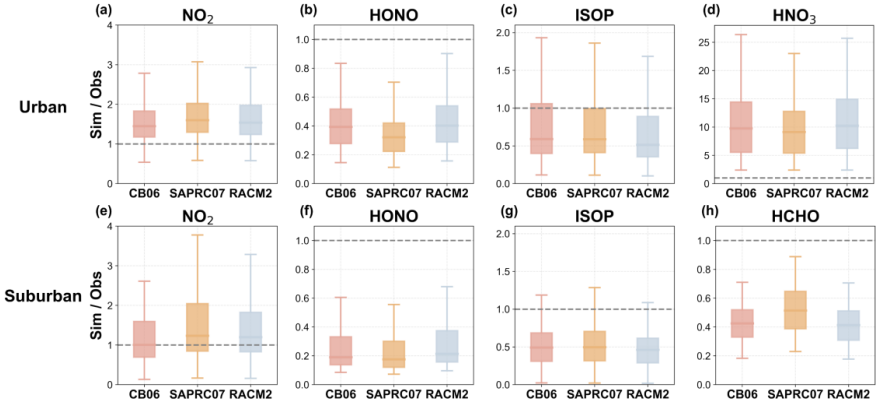

Figure 4 Comparison of three photochemical mechanisms on key photochemical species at urban site and suburban site. The box plots present the 10th, 25th, 50th, 75th, and 90th percentiles of the ratio of Simulation value vs Observation value (08:00–18:00 local time) individually.

The accuracy of simulation key photochemical species such as NO_2, HONO, ISOP, HCHO, and HNO_3 is also one of the critical factors in evaluating the ability of different photochemical mechanisms, particularly under varying NO_x concentrations. On the whole, all the three photochemical mechanisms significantly overestimated daytime NO_2 concentrations at the urban site. At the suburban site, while SAPRC07 and RACM2 continued to exhibit notable overestimations, CB06 demonstrated superior agreement with observations (Fig. 4a, e). Specifically, at the urban site, the median simulated-to-observed NO_2 ratios for SAPRC07, RACM2, and CB06 were 1.60, 1.54, and 1.46, respectively. In contrast, at the suburban site, SAPRC07 and RACM2 maintained high biases with median ratios of 1.24 and 1.20, whereas CB06 yielded a near-perfect ratio of 1.01. The overestimation NO_2 at the urban site in Chengdu is consistent with the findings of She et al. (2024). The possible reasons might be attributed that overestimation of NO_2 emission (Du et al., 2021) or inadequate representation of NO_2 recycling pathways in the model (Luecken et al., 2019).

https://doi.org/10.5194/egusphere-2026-1786
Preprint. Discussion started: 30 April 2026

As a vital precursor to OH radicals, HONO plays a central role in driving secondary atmospheric pollution. Thus, its accurate simulation is essential for air quality models (Tan et al., 2017; Tan et al., 2026). Contrary to the simulated NO_2 concentrations, all the three photochemical mechanisms significantly underestimated HONO concentrations at both urban and suburban sites (Fig. 4b, f). The underestimation may be related to missing HONO sources in the current modeling framework, which may include direct emissions (e.g., soil emissions (Wang et al., 2021; Wang et al., 2025b), vehicles (Trinh et al., 2017) and biomass combustion (Cui et al., 2021)), heterogeneous processes (e.g., heterogeneous reactions of NO_2 on aerosols and ground (Xuan et al., 2025; Zhang et al., 2021)) and nitrate photolysis (Scharko et al., 2014; Ye et al., 2017). Notably, while the underestimations were particularly pronounced at the suburban site, inter-mechanistic discrepancies were more significant in the urban environment. Specifically, the median ratios of simulated-to-observed HONO at the urban site were 0.40 (RACM2), 0.38 (CB06) and 0.32 (SAPRC07), whereas at the suburban site, they dropped to 0.21, 0.19, and 0.18, respectively. Though RACM2 demonstrated the relatively best performance in simulating HONO among the three schemes, the results underscore the urgent need for refined HONO-related chemical mechanisms within CMAQ.

We further evaluated the simulation performance of ISOP, a key precursor originating from BVOC, across the three mechanisms. Similar to the trends observed for HONO, all the three chemical mechanisms systematically underestimated ISOP concentrations at both sites (Fig. 4c, g), with pronounced negative biases occurring in the suburban environment. These discrepancies likely stem from a combination of factors, including the underestimation of anthropogenic isoprene sources (e.g., vehicle isoprene emission (Park et al., 2011)), coarse-resolution land-use data affecting biogenic emission modelling (Wang et al., 2025a), and inherent uncertainties in ISOP-related oxidation chemistry (Von Kuhlmann et al., 2004).

HNO_3 is a primary product of radical chain termination, particularly in high-NO_x environments. Overall, the simulated HNO_3 concentrations across all three chemical mechanisms were anomalously higher than observations at the urban site, with median simulated-to-observed ratios ranging from 9.13 to 10.27. The RACM2 exhibited the most pronounced bias, yielding a median ratio of 10.27 (Fig. 4d). The overestimations are likely attributed to the previously noted overestimation of NO_2 concentrations, which enhances the OH + NO_2 reaction and subsequently accelerates the production of HNO_3.

https://doi.org/10.5194/egusphere-2026-1786
Preprint. Discussion started: 30 April 2026

Regarding HCHO, which is primarily derived from the photooxidation of VOC, all three mechanisms systematically underestimated HCHO concentrations at the suburban site. As HCHO photolysis serves as a major source of radicals, its accurate simulation is vital for characterizing atmospheric oxidation capacity. A comparison of the three schemes reveals that SAPRC07 showed the best agreement with observations, whereas RACM2 and CB06 exhibited similarly pronounced underestimations. These findings align with previous studies suggesting that various mechanisms, including CB05 and MCM, often underestimate HCHO due to uncertainties in their isoprene oxidation schemes (Marvin et al., 2017). Notably, the superior performance of SAPRC07 in simulating HCHO peaks at the suburban site corresponds directly to its higher simulated concentrations of radicals compared to the other two mechanisms.

3.1.3 Comparisons in spatial-temporal RO_x Radicals

OH, HO_2, and RO_2 radicals (collectively RO_x) serve as key oxidizing agents in the atmosphere, and their concentrations are fundamental indicators of atmospheric oxidation capacity. The RO_x radicals cycle generates HO_2 and RO_2, facilitating NO oxidation to NO_2 and further driving O_3 production. To evaluate the simulation performance of the CB06, SAPRC07, and RACM2 mechanisms, we quantified the spatial distribution of radicals across the region and analyzed the diurnal variations of and concentrations at the XJ site (Fig. 5).

https://doi.org/10.5194/egusphere-2026-1786
Preprint. Discussion started: 30 April 2026

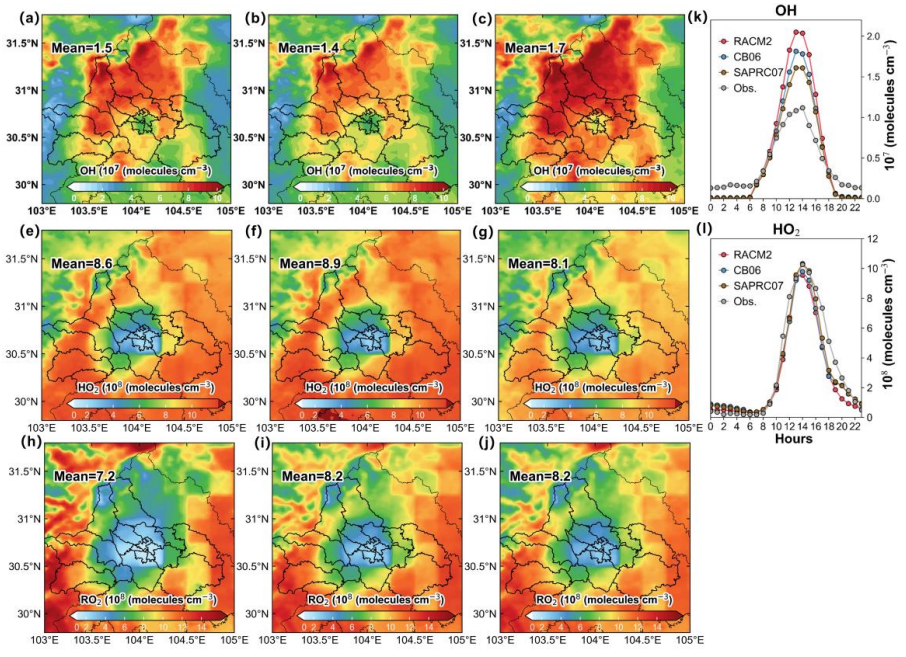

Figure 5 Regional distributions of OH, HO_2 and RO_2 radical concentration at 12:00 local time and diurnal variation at XJ site of OH and HO_2 concentration simulated by three photochemical mechanisms during August 9-August 18, 2019.

Generally, the spatial distribution of OH, HO_2 and RO_2 radical concentrations simulated by the three chemical mechanisms are largely consistent (Fig. 5). For specific, the high-value region of OH radical concentrations across Chengdu region are mainly concentrated around the main urban area, while the a low-value region in the urban center. The response characteristics of OH radical to NO_x concentrations are consistent with the distinct response patterns of OH concentration to varying NO levels across urban, forest, and marine environments revealed by Tan et al. (2026). The low OH concentration zone in heavily polluted urban may result from the reaction of OH radical and NO_2, which is a important loss process for OH radicals in urban (Ehhalt et al., 1990). Different from the spatial pattern of OH radicals, there was a notable low-value area of HO_2 radical in the central urban area of Chengdu, while high-value area of that in most surrounding areas. The low-value area in the central urban may be attributed to high NO emissions. Under the conditions of high NO concentration, the reaction between NO and HO_2 radicals is the dominant reaction pathway for HO_2 (Tang et al., 2006). And this reaction could lead to rapid

https://doi.org/10.5194/egusphere-2026-1786
Preprint. Discussion started: 30 April 2026

consumption of HO_2 radicals, resulting in lower HO_2 concentrations in urban areas compared to suburban areas. Across all three mechanisms, the spatial distribution of RO_2 radicals closely mirrors that of HO_2. Despite generally consistent spatial patterns, significant quantitative discrepancies exist among the three mechanisms regarding radical concentrations and their simulation performance. For OH radicals, the RACM2 simulated a regional mean concentration of 1.7×10^7 molecules cm^{-3}, notably higher than the 1.4×10^7 molecules cm^{-3} predicted both by SAPRC07 and CB06. Diurnal profiles at the XJ site further confirm that RACM2 produces higher peaks than the other two schemes. While literature suggests that CBM and SAPRC mechanisms tend to underestimate OH radical relative to RACM2 (Liu et al., 2023), our comparison with in-situ observations at the XJ site reveals that all three mechanisms significantly overestimated peak levels, with RACM2 exhibiting the most pronounced positive bias.

In contrast, SAPRC07 yielded the highest daytime HO_2 peaks at the XJ site, corresponding to the simulated HCHO peaks (Fig. 4). This superior HCHO performance corresponds directly to SAPRC07 simulating the highest regional mean HO_2 concentration (8.9×10^8 molecules cm^{-3}), followed by CB06 (8.6×10^8 molecules cm^{-3}) and RACM2 (8.1×10^8 molecules cm^{-3}). Notably, the CB06 mechanism produced a regional mean RO_2 concentration of only 7.2×10^8 molecules cm^{-3}, which is significantly lower than the 8.2×10^8 molecules cm^{-3} simulated by both RACM2 and SAPRC07. These inter-mechanistic discrepancies in radical levels were most concentrated in the high-NO_x urban core, which ultimately explains why CB06 yields the lowest overall O_3 simulation values.

https://doi.org/10.5194/egusphere-2026-1786
Preprint. Discussion started: 30 April 2026

3.2 Budget Analysis of O_3 Production and Loss Pathways

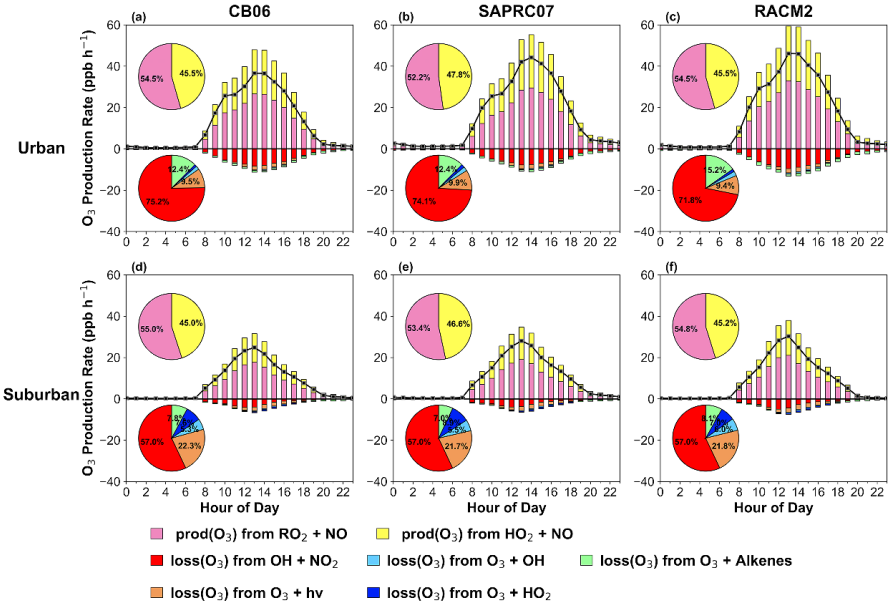

Figure 6 Reaction rates (ppbv/h) of various production and loss pathways of O_3 simulated by three photochemical mechanisms during daytime (08:00 – 18:00 local time). The black curve plotted with square markers shows the net O_3 production rate.

To analyze mechanistic discrepancies in formation, we evaluated mean diurnal reaction rates for production and loss pathways (Fig. 6). Across both sites, the net production rate ($P(O_3)$) and key formation pathways (RO_2 + NO and HO_2+NO) followed a consistent hierarchy: RACM2 > SAPRC07 > CB06. Specifically, $P(O_3)$ values for RACM2, SAPRC07, and CB06 were 31.0, 29.6, and 25.0 ppbv/h at the urban site, and 17.6, 17.4, and 15.1 ppbv/h at the suburban site, respectively. This ranking was mirrored in the individual reaction rates; for instance, urban RO_2+NO rates ranged from 17.8 to 22.0 ppbv/h, while HO_2 +NO rates ranged from 14.7 to 18.1 ppbv/h. Notably, inter-mechanistic budget discrepancies were more pronounced in the high-NO_x urban environment than in the suburban setting. Although the $P(O_3)$ and the individual reaction rates of specific O_3 production and loss pathways differed across the three mechanisms, the main O_3 production and loss pathways were generally consistent. At both sites, the O_3 production pathway was dominated by the RO_2+NO reaction, accounted for over 50%. However, there were significant differences in O_3 loss pathways between urban and suburban areas. In urban areas with high-NO_x environment, O_3 loss was primarily dominated by the OH+NO_2 reaction, with

https://doi.org/10.5194/egusphere-2026-1786
Preprint. Discussion started: 30 April 2026

406 contribution ratios ranging from 71.8% ~ 75.2%, followed by the O_3+Alkenes (12.4%–15.2%) and the
407 O_3+hv (9.4%–9.5%). And the contributions from the remaining pathways are negligible. At the suburban
408 site with low-NO_x environment, although the OH+NO_2 reaction still dominated the loss of O_3, its
409 contribution decreased by nearly 20% and the contributions of the O_3+hv (21.7%–22.3%), O_3+HO_2
410 (7.0%–8.9%), and O_3+OH reactions (5.3%–6.0%) increase significantly.

411 **3.3 Mechanistic insights into RO_x radical cycle**

412 **3.3.1 Characterizing primary sources of RO_x radicals**

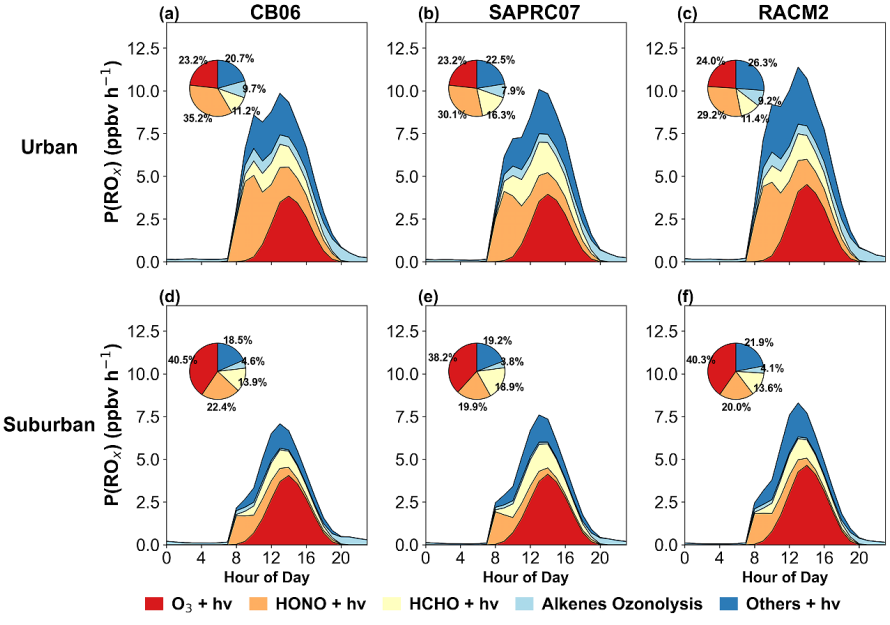

413

414 **Figure 7 Primary sources for RO_x radicals simulated by three photochemical mechanisms at urban site (SAES)**
415 **and suburban site (XJ) during the ozone (O_3) pollution episode include: HONO photolysis, O_3 photolysis,**
416 **alkene ozonolysis, HCHO photolysis and other Carbonyls photolysis.**

417 The interactions between the NOx cycle and the RO_x cycle continuously generate HO_2 and RO_2, thereby
418 facilitating the conversion of NO to NO_2 and contributing to the gradual accumulation of O_3. Therefore,
419 quantifying the budget and cycle of RO_x radicals is essential for elucidating changes in atmospheric
420 oxidation capacity and the mechanisms of O_3 formation in different photochemical mechanisms. Here,
421 we analyzed the primary sources of RO_x radicals at both sites (Fig. 7). These results demonstrated the
422 production rates of primary RO_x radical ($P(RO_x)$) at the urban site were significantly higher at the
423 suburban site, with RACM2 consistently simulated the highest reaction rates in both environments.

https://doi.org/10.5194/egusphere-2026-1786
Preprint. Discussion started: 30 April 2026

Moreover, the three mechanisms exhibited considerable divergence in $P(RO_x)$ under high-NO_x urban conditions, whereas these yield more consistent results in the low-NOx suburban environment.

Consistent with the budget findings, all three mechanisms identify the same predominant drivers of $P(RO_x)$ across both urban and suburban environments. In the high-NO_x urban setting, HONO photolysis is the primary driver of $P(RO_x)$ whereas O_3 photolysis dominates in the low-NO_x suburban environment. In specific, at the urban site, HONO photolysis with a contribution rate of 29.2% ~ 35.2% contributed the highest proportion to $P(RO_x)$, which is consistent with the results of Chengdu in Zhou's research (Zhou et al., 2024). And it was followed by O_3 photolysis (23.2% ~ 24.0%) or photolysis of other carbonyl compounds (20.7% ~ 26.3%). The remaining production was attributed to HCHO photolysis (11.2% ~ 16.3%), and the oxidation reactions between O_3 and Alkenes (7.9% ~ 9.7%). The contribution of photolysis of other carbonyls to the primary RO_x source simulated by the RACM2 mechanism was significantly higher than that of the other two mechanisms, which may be due to differences in the photolysis rate parameters of hydroxyl compounds, such as absorption cross-sections and quantum yields. At the suburban site, the highest contribution ratio to the $P(RO_x)$ originated from O_3+hv (38.2%–40.5%), followed by HONO photolysis (19.9%–22.4%) or photolysis of other carbonyls (18.5%–21.9%), while HCHO photolysis and the oxidation reactions between O_3 and alkenes accounted for 13.6%~18.9% and 3.8%~4.6%, respectively.

https://doi.org/10.5194/egusphere-2026-1786
Preprint. Discussion started: 30 April 2026

3.3.2 Termination mechanisms and radical fate in urban and suburban environments

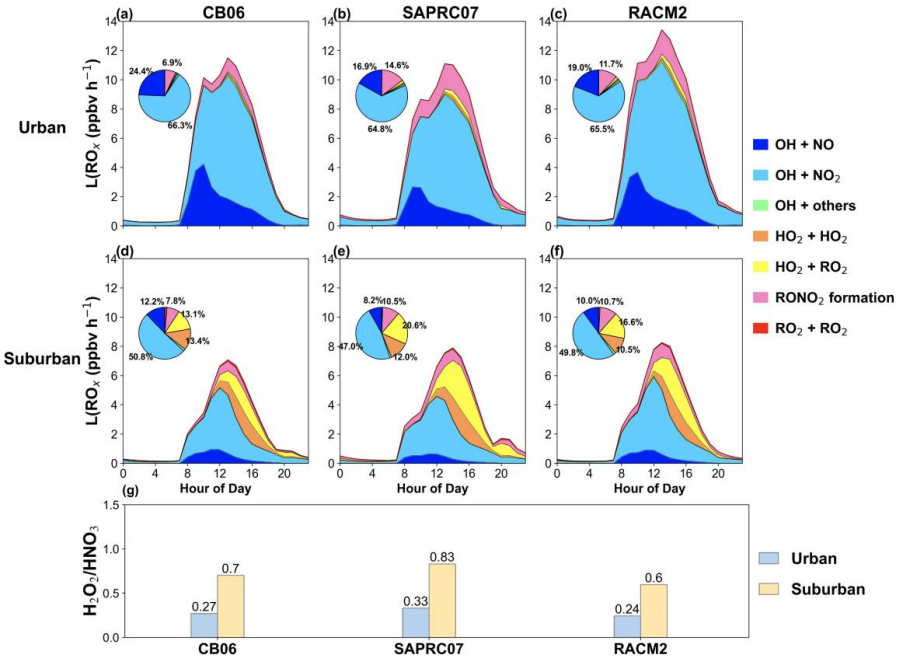

Figure 8 Diurnal variations in radical chain termination for RO_x cycle (a-f) and daytime (08:00 – 18:00) H_2O_2-to-HNO_3 ratio (g) simulated by three photochemical mechanisms at urban site (SAES) and suburban site (XJ) during the O_3 pollution episode.

We further quantified the termination reaction rates of the RO_x radical chain at both sites (Fig. 8). Overall, all the three mechanisms consistently simulated substantially higher RO_x loss ($L(RO_x)$) rates at the urban site than that at the suburban site. The radical terminations were mainly driven by the reactions forming HNO_3 ($OH+NO_2$, 64.8% ~ 66.3%) and organic nitrates ($RONO_2$) (16.9% ~ 24.4%) at the high-NO_x urban site, whereas HO_2+RO_2, HO_2+HO_2, and RO_2+RO_2 reactions were more important at the low-NO_x suburban site (Fig. 7). Previous work also reported that the OH-HO_2-RO_2 radical system termination in Chengdu was dominated by the OH + NO_x reaction(Tan et al., 2018). At the suburban site, although the highest contribution to $L(RO_x)$ among various reaction pathways was still from $OH+NO_2$ (47.0% ~ 50.8%), this contribution decreased significantly by nearly 20%, while the contributions of other reaction pathways to $L(RO_x)$ increased, such as HO_2+RO_2 (13.1% ~ 20.6%), HO_2+HO_2 (10.5% ~ 13.4%), and RO_2+RO_2 (7.8% ~ 10.7%). This shift of dominant pathways for RO_x radical chain termination from urban to suburban was further supported by the H_2O_2/HNO_3 ratio which is the terminated product of the RO_x cycle. It rose significantly from 0.31 ~ 0.41 at urban site to 0.76 ~ 1.0 at suburban site (Fig. 8g).

https://doi.org/10.5194/egusphere-2026-1786
Preprint. Discussion started: 30 April 2026

The shift in RO_x termination chemistry from urban to suburban conditions reflects a systematic transition in photochemical regimes, governed by NO_x availability and radical cycling efficiency. The predominance of OH + NO_2 and $RONO_2$ formation at the urban site reflects strong radical sequestration under high-NO_x conditions, limiting RO_x recycling and constraining O_3 production efficiency. Such a chemical environment is indicative of a VOC-limited regime, in which O_3 formation is more sensitive to VOC availability than to further reductions in NO_x. In contrast, the increased importance of peroxyl radical reactions at the suburban site suggests a more efficient radical propagation environment under lower NO_x levels. The enhanced contributions of HO_2 + HO_2 and HO_2+ RO_2, together with the elevated H_2O_2/HNO_3 ratio, point to a transition or a NO_x-limited regime.

3.3.3 Propagation pathways: OH-initiated oxidation of primary VOC emission

The RO_x radical cycle is typically initiated by the OH-induced oxidation of VOC, which generates RO_2 radicals and trigger a sequence of propagation reactions. These propagation steps, specifically the reactions of RO_2 and HO_2 with NO, facilitate the catalytic conversions of NO to NO_2, there by leading to the accumulation of O_3. In order to identify the key chemical drivers of the RO_x cycle across varying NO_x environments, we quantified the reaction rates of OH with major primary VOC emissions at urban and suburban site (Fig. 9).

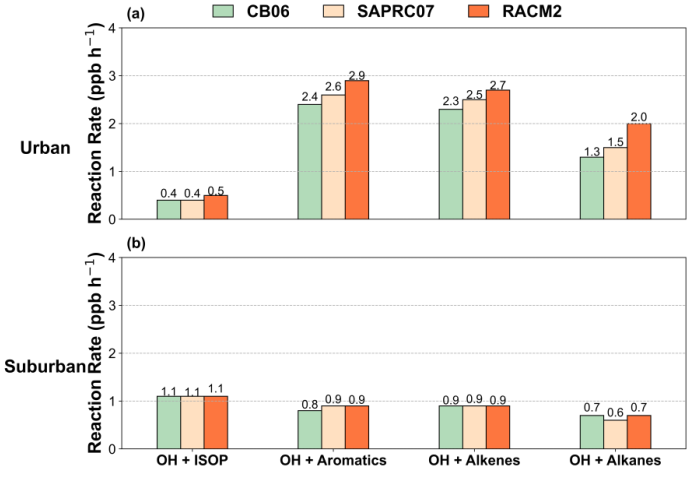

Figure 9 Reaction rates (ppbv/h) of OH radical with major primary VOC simulated by three photochemical mechanisms at urban site (SAES) and suburban site (XJ) during daytime (08:00 – 18:00 local time).

https://doi.org/10.5194/egusphere-2026-1786
Preprint. Discussion started: 30 April 2026

Alkanes represent the most abundant VOC class in Chengdu, while alkenes and aromatics are the primary high-reactivity components of anthropogenic emissions (Deng et al., 2019; Tan et al., 2018). Furthermore, ISOP is a critical BVOC species. Consequently, this study quantified the OH-initiated reaction rates of these key anthropogenic and biogenic VOC to evaluate their respective roles in driving the RO_x cycle. Across all the three mechanisms, the reaction rates between OH and primary VOC emission were consistently higher at the urban site compared to the suburban site, revealing that urban areas have a greater capacity for secondary pollutant formation. Moreover, the RO_x cycle at the high-NO_x urban site was primarily driven by OH reactions with anthropogenic VOC (AVOC), with aromatics and alkenes serving as the dominant chemical drivers. In contrast, at the low-NO_x suburban site, it was mainly driven by OH reactions with BVOC such as isoprene, although AVOC continued to play a significant role.

Although the three mechanisms exhibited a consistent understanding of the reaction rates between OH and key primary VOC emissions, quantitative discrepancies exist. At the urban site, these rates followed the hierarchy of RACM2 > SAPRC07 > CB06, while the differences are relatively smaller at the suburban site. Notably, the minimum reactivity simulated by CB06 aligns with its lower radical concentrations previously identified in Section 3.1. In addition, the reaction rates of OH with different primary VOC emissions simulated by the three mechanisms also exhibited slight differences. Furthermore, the initial OH reaction rate alone cannot fully capture the relative importance of different VOC classes to O_3 production. For instance, aromatics undergo multi-stage oxidation that continuously regenerates RO_2 and HO_2 radicals, meaning their total impact on O_3 formation cannot be quantified solely by their initial reaction with OH. Consequently, a more rigorous evaluation of precursor sensitivity is required to assess the contribution of various categories, as discussed in Section 3.4.

https://doi.org/10.5194/egusphere-2026-1786
Preprint. Discussion started: 30 April 2026

3.4 Sensitivity of O_3 to NO_x and VOC emissions

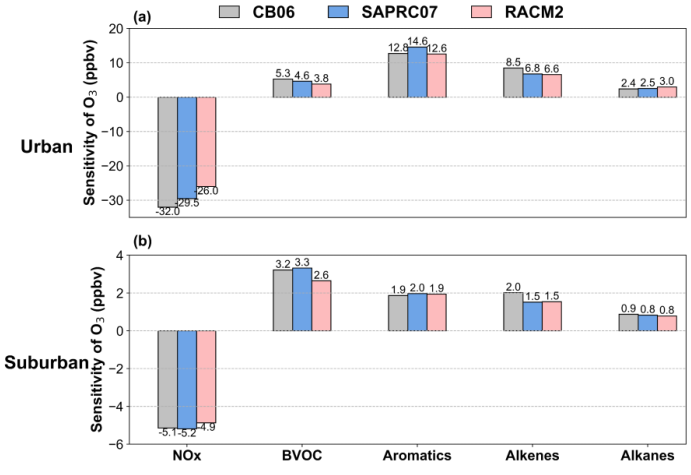

Figure 10 Sensitivity coefficients of daytime O_3 concentrations to primary NO_x emissions and key primary VOC emissions at urban and suburban sites simulated by CMAQ-DDM under three photochemical mechanisms.

Reaction rates between primary VOC emissions and OH radicals alone cannot fully capture their contributions to atmospheric oxidation capacity and O_3 formation. Therefore, a more comprehensive quantitative analysis is required to identify key precursor emissions. Here, we quantify the sensitivity of O_3 production to anthropogenic emissions (NO_x, aromatics, alkenes, and alkanes) and BVOCs using the CMAQ-DDM module across the three mechanisms (Fig. 10). Overall, the three chemical mechanisms produced consistent patterns in O_3 sensitivity to NO_x and major VOC groups, although the absolute magnitudes differed. Anthropogenic aromatics and alkenes dominated O_3 formation at the urban site, whereas BVOCs were the primary contributors at the suburban site, with alkanes consistently showing the lowest sensitivity. At the urban site, the first-order sensitivity coefficients of O_3 were 12.6–14.6 ppbv for aromatics, 6.6–8.5 ppbv for alkenes, 3.8–5.3 ppbv for BVOCs, and 2.3–3.0 ppbv for alkanes. In contrast, at the suburban site, O_3 showed the highest sensitivity to BVOCs (2.6–3.3 ppbv), followed by aromatics (1.9–2.0 ppbv) and alkenes (1.5–2.0 ppbv), while alkanes remained the least influential (0.8–0.9 ppbv).

Notably, despite the higher OH reactivity of ISOP at the suburban site (Fig. 9), the first-order sensitivity of O_3 to BVOC was greater at high-NO_x urban site. This apparent discrepancy reflects differences in radical fate under contrasting NOx regimes. Under high-NO_x urban conditions, RO_2 and HO_2 radicals

https://doi.org/10.5194/egusphere-2026-1786
Preprint. Discussion started: 30 April 2026

from ISOP oxidation reacted more efficiently with NO, promoting the conversion of NO to NO_2 and net O_3 production. In contrast, under low-NO_x suburban conditions, these radicals are more likely to undergo RO_2+RO_2, RO_2+HO_2, and HO_2+HO_2 reactions, forming organic peroxides and terminating the radical chain (Fig. 8). This shift reduces O_3 production efficiency and can even suppress net O_3 formation, further highlighting the amplified impact of BVOC emissions on O_3 production under high-NO_x conditions.

4 Conclusions and implications

This study developed a customized VOC emission inventory for RACM2 and conducted a systematic inter-comparison of three photochemical mechanisms (CB06, SAPRC07, and RACM2) using CMAQ during an O_3 pollution episode in Chengdu under contrasting NOx environments. The results show that chemical mechanism selection leads to substantial differences in simulated O_3 levels and radical chemistry, particularly under high-NO_x conditions.

While SAPRC07 and RACM2 simulated higher and comparable O_3 concentrations (~95 ppbv) than CB06 (~80 ppbv), all three mechanisms consistently reproduced the fundamental photochemical process of O_3 formation. In particular, O_3 production was dominated by the RO_2 + NO pathway, and the RO_x cycle exhibited a clear transition in termination chemistry from urban to suburban environments. At the urban site, radical termination was primarily controlled by OH + NO_2, whereas at the suburban site, radical self- and cross-reactions became increasingly important. This transition was further reflected by the increase in the H_2O_2/HNO_3 ratio from ~0.3 in urban areas to ~1.0 in suburban regions, indicating a shift from VOC-limited to NO_x-limited regimes. Sensitivity analysis revealed a consistent but regime-dependent pattern of precursor control. Anthropogenic aromatics and alkenes dominated O_3 formation in urban areas, whereas BVOCs became the primary drivers in suburban environments. Notably, O_3 sensitivity to BVOCs remained substantial under high-NO_x urban conditions, despite lower BVOC emissions. This reflects the enhanced efficiency of RO_2 + NO reactions, which promote radical recycling and amplify the contribution of BVOCs to O_3 production.

Overall, these findings highlight that chemical mechanism uncertainty is strongly dependent on NO_x regimes and is most pronounced under high-NO_x conditions, underscoring the need for multi-mechanism ensemble simulations in air quality modeling. Furthermore, the clear urban–suburban contrast in O_3 formation regimes suggests that emission control strategies should be spatially differentiated, with VOC reductions prioritized in urban cores and NO_x controls more effective in suburban and downwind regions. Importantly, NO_x not only directly regulates O_3 formation but also modulates radical cycling and thus

https://doi.org/10.5194/egusphere-2026-1786
Preprint. Discussion started: 30 April 2026

the effectiveness of VOC emissions, which should be explicitly considered in control strategies. Finally, the amplified role of BVOC under high-NO_x conditions highlights the importance of accounting for interactions between anthropogenic emissions and biogenic sources in future O_3 mitigation, particularly under a warming climate with increasing BVOC emissions.

Author contributions

LYL and GYJ contributed equally to this work. LYL conducted the model simulations, performed data analysis, prepared the figures, and wrote original draft with contributions from all coauthors. WN and LKD contributed to the writing and revision of the manuscript. GYJ, WN, LKD, ZYH, GYJ, SGM and YFM designed the research. LKD, ZYH and GYJ provided the observation data support. SGM and YFM provided computing resources and assisted in conducting the model simulations.

Competing interests

The contact author has declared that none of the authors has any competing interests.

Disclaimer

Publisher's note: Copernicus Publications remains neutral with regard to jurisdictional claims made in the text, published maps, institutional affiliations, or any other geographical representation in this paper. The authors bear the ultimate responsibility for providing appropriate place names. Views expressed in the text are those of the authors and do not necessarily reflect the views of the publisher.

Acknowledgements

This research was supported by the National Key Research and Development Program of China(2023YFC3706100， 2023YFC3709304), National Natural Science Foundation of China (42575120).

https://doi.org/10.5194/egusphere-2026-1786
Preprint. Discussion started: 30 April 2026

Financial support

This research was supported by the National Key Research and Development Program of China(2023YFC3706100， 2023YFC3709304), National Natural Science Foundation of China (42575120).

References

Ashmore, M. R.: Assessing the future global impacts of ozone on vegetation, Plant, Cell & Environment, 28, 949-964, https://doi.org/10.1111/j.1365-3040.2005.01341.x, 2005.

Byun, D. and Schere, K. L.: Review of the governing equations, computational algorithms, and other components of the models-3 Community Multiscale Air Quality (CMAQ) modeling system, APPLIED MECHANICS REVIEWS, 59, 51-77, 10.1115/1.2128636, 2006.

Carter, W. P. L.: Condensed atmospheric photooxidation mechanisms for isoprene, Atmospheric Environment, 30, 4275-4290, https://doi.org/10.1016/1352-2310(96)00088-X, 1996.

Cordiner, S., Baciocchi, R., and Attinà, M.: A sensitivity analysis of ozone formation to ambient air composition by means of photochemical models, URBAN AIR QUALITY - RECENT ADVANCES, PROCEEDINGS, WOS:000181346400041200 2.

Cui, L. L., Li, R., Fu, H. B., Meng, Y., Zhao, Y. L., Li, Q., and Chen, J. M.: Nitrous acid emission from open burning of major crop residues in mainland China, ATMOSPHERIC ENVIRONMENT, 244, 10.1016/j.atmosenv.2020.117950, 2021.

Deng, Y. Y., Li, J., Li, Y. Q., Wu, R. R., and Xie, S. D.: Characteristics of volatile organic compounds, NO2, and effects on ozone formation at a site with high ozone level in Chengdu, JOURNAL OF ENVIRONMENTAL SCIENCES, 75, 334-345, 10.1016/j.jes.2018.05.004, 2019.

Dodge, M. C.: Chemical oxidant mechanisms for air quality modeling: critical review, Atmospheric Environment, 34, 2103-2130, https://doi.org/10.1016/S1352-2310(99)00461-6, 2000.

Du, Y., Huang, R., Wang, X., Qin, M., Zhang, W., Zhang, Y., Yang, Y., Zhang, W., Luo, B., Hu, Y., and Russell, A. G.: Implementing Reduced Form Model to Construct Ozone Isopleths and Its Application, Acta Scientiarum Naturalium Universitatis Pekinensis, 57, 311-321, 10.13209/j.0479-8023.2020.120, 2021.

Dunker, A. M.: The decoupled direct method for calculating sensitivity coefficients in chemical kinetics, The Journal of Chemical Physics, 81, 2385-2393, 10.1063/1.447938, 1984.

Dunker, A. M., Yarwood, G., Ortmann, J. P., and Wilson, G. M.: The Decoupled Direct Method for Sensitivity Analysis in a Three-Dimensional Air Quality Model Implementation, Accuracy, and Efficiency, Environmental Science & Technology, 36, 2965-2976, 10.1021/es0112691, 2002.

Ehhalt, D. H., Dorn, H. P., and Poppe, D.: The chemistry of the hydroxyl radical in the troposphere, Proceedings of the Royal Society of Edinburgh. Section B. Biological Sciences, 97, 17-34, 10.1017/S0269727000005273, 1990.

Friedlander, S. K. and Seinfeld, J. H.: Dynamic model of photochemical smog, Environmental Science & Technology, 3, 1175-1181, 10.1021/es60034a003, 1969.

Fu, X., Wang, T., Gao, J., Wang, P., Liu, Y., Wang, S., Zhao, B., and Xue, L.: Persistent Heavy Winter Nitrate Pollution Driven by Increased Photochemical Oxidants in Northern China, Environmental Science & Technology, 54, 3881-3889, 10.1021/acs.est.9b07248, 2020.

https://doi.org/10.5194/egusphere-2026-1786
Preprint. Discussion started: 30 April 2026

611 Geng, G., Liu, Y., Liu, Y., Liu, S., Cheng, J., Yan, L., Wu, N., Hu, H., Tong, D., Zheng, B., Yin, Z., He,
612 K., and Zhang, Q.: Efficacy of China's clean air actions to tackle PM2.5 pollution between 2013 and
613 2020, Nature Geoscience, 17, 987-994, 10.1038/s41561-024-01540-z, 2024.
614 Goliff, W. S., Stockwell, W. R., and Lawson, C. V.: The regional atmospheric chemistry mechanism,
615 version 2, Atmospheric Environment, 68, 174-185, https://doi.org/10.1016/j.atmosenv.2012.11.038,
616 2013.
617 Guenther, A. B., Jiang, X., Heald, C. L., Sakulyanontvittaya, T., Duhl, T., Emmons, L. K., and Wang, X.:
618 The Model of Emissions of Gases and Aerosols from Nature version 2.1 (MEGAN2.1): an extended and
619 updated framework for modeling biogenic emissions, Geosci. Model Dev., 5, 1471-1492, 10.5194/gmd-
620 5-1471-2012, 2012.
621 Han, H., Zhang, L., Wang, X. L., and Lu, X.: Contrasting Domestic and Global Impacts of Emission
622 Reductions in China on Tropospheric Ozone, JOURNAL OF GEOPHYSICAL RESEARCH-
623 ATMOSPHERES, 129, 10.1029/2024JD041453, 2024.
624 Hofzumahaus, A., Brauers, T., Platt, U., and Callies, J.: LATITUDINAL VARIATION OF MEASURED
625 O-3 PHOTOLYSIS FREQUENCIES J(O1D) AND PRIMARY OH PRODUCTION-RATES OVER
626 THE ATLANTIC-OCEAN BETWEEN 50-DEGREES-N AND 30-DEGREES-S, JOURNAL OF
627 ATMOSPHERIC CHEMISTRY, 15, 283-298, 10.1007/BF00115399, 1992.
628 Huang, L., Liu, H., Yarwood, G., Wilson, G., Tao, J., Han, Z., Ji, D., Wang, Y., and Li, L.: Modeling of
629 secondary organic aerosols (SOA) based on two commonly used air quality models in China: Consistent
630 S/IVOCs contribution but large differences in SOA aging, Science of The Total Environment, 903,
631 166162, https://doi.org/10.1016/j.scitotenv.2023.166162, 2023.
632 Huang, L., Zhang, X., Emery, C., Mu, Q., Yarwood, G., Zhai, H., Sun, Z., Xue, S., Wang, Y., Fu, J. S.,
633 and Li, L.: Recommendations on benchmarks for numerical air quality model applications in China –
634 Part 2: Ozone and uncertainty analysis, Atmos. Chem. Phys., 25, 4233-4249, 10.5194/acp-25-4233-2025,
635 2025.
636 Huang, X., Ding, A., Gao, J., Zheng, B., Zhou, D., Qi, X., Tang, R., Wang, J., Ren, C., Nie, W., Chi, X.,
637 Xu, Z., Chen, L., Li, Y., Che, F., Pang, N., Wang, H., Tong, D., Qin, W., Cheng, W., Liu, W., Fu, Q., Liu,
638 B., Chai, F., Davis, S. J., Zhang, Q., and He, K.: Enhanced secondary pollution offset reduction of primary
639 emissions during COVID-19 lockdown in China, National Science Review, 8, nwaa137,
640 10.1093/nsr/nwaa137, 2021.
641 Jenkin, M. E., Young, J. C., and Rickard, A. R.: The MCM v3.3.1 degradation scheme for isoprene,
642 Atmos. Chem. Phys., 15, 11433-11459, 10.5194/acp-15-11433-2015, 2015.
643 Kitayama, K., Morino, Y., Yamaji, K., and Chatani, S.: Uncertainties in O3 concentrations simulated by
644 CMAQ over Japan using four chemical mechanisms, Atmospheric Environment, 198, 448-462,
645 https://doi.org/10.1016/j.atmosenv.2018.11.003, 2019.
646 Kuai, L., Bowman, K. W., Worden, H. M., Herman, R. L., and Kulawik, S. S.: Hydrological controls on
647 the tropospheric ozone greenhouse gas effect, ELEMENTA-SCIENCE OF THE ANTHROPOCENE, 5,
648 10.1525/elementa.208, 2017.
649 Li, F., Newman, P., Pawson, S., and Perlwitz, J.: Effects of Greenhouse Gas Increase and Stratospheric
650 Ozone Depletion on Stratospheric Mean Age of Air in 1960-2010, JOURNAL OF GEOPHYSICAL
651 RESEARCH-ATMOSPHERES, 123, 2098-2110, 10.1002/2017JD027562, 2018.
652 Li, J., Huang, J., Huang, Y., Liu, C., Zhang, X., Chen, Y., Cheung, V. T. F., Sobnack, M. B., and Fung, J.:
653 Improving ozone episode predictions in the Great Bay Area: An evaluation of the contribution of gas-

https://doi.org/10.5194/egusphere-2026-1786
Preprint. Discussion started: 30 April 2026

phase chemical mechanisms, Atmospheric Environment: X, 28, 100392, https://doi.org/10.1016/j.aeaoa.2025.100392, 2025a.

Li, M., Liu, H., Geng, G. N., Hong, C. P., Liu, F., Song, Y., Tong, D., Zheng, B., Cui, H. Y., Man, H. Y., Zhang, Q., and He, K. B.: Anthropogenic emission inventories in China: a review, NATIONAL SCIENCE REVIEW, 4, 834-866, 10.1093/nsr/nwx150, 2017.

Li, M., Chen, S., Jiang, X., Ye, L., Guo, Y., Li, W., Zhang, J., Liu, W., Yang, Y., Ou, Z., Chen, L., Dong, G., Wu, W., Li, D., and Chen, W.: Subchronic ozone exposure leads to multi-organ injuries with differential reversibility in male C57BL/6 J mice, Journal of Hazardous Materials, 492, 138049, https://doi.org/10.1016/j.jhazmat.2025.138049, 2025b.

Liu, X. H., Zhang, Y., Xing, J., Zhang, Q. A., Wang, K., Streets, D. G., Jang, C., Wang, W. X., and Hao, J. M.: Understanding of regional air pollution over China using CMAQ, part II. Process analysis and sensitivity of ozone and particulate matter to precursor emissions, ATMOSPHERIC ENVIRONMENT, 44, 3719-3727, 10.1016/j.atmosenv.2010.03.036, 2010.

Liu, Y., Li, J., Ma, Y., Zhou, M., Tan, Z., Zeng, L., Lu, K., and Zhang, Y.: A review of gas-phase chemical mechanisms commonly used in atmospheric chemistry modelling, Journal of Environmental Sciences, 123, 522-534, https://doi.org/10.1016/j.jes.2022.10.031, 2023.

Liu, Y. M. and Wang, T.: Worsening urban ozone pollution in China from 2013 to 2017-Part 2: The effects of emission changes and implications for multi-pollutant control, ATMOSPHERIC CHEMISTRY AND PHYSICS, 20, 6323-6337, 10.5194/acp-20-6323-2020, 2020.

Lu, K. D., Rohrer, F., Holland, F., Fuchs, H., Bohn, B., Brauers, T., Chang, C. C., Häseler, R., Hu, M., Kita, K., Kondo, Y., Li, X., Lou, S. R., Nehr, S., Shao, M., Zeng, L. M., Wahner, A., Zhang, Y. H., and Hofzumahaus, A.: Observation and modelling of OH and HO₂ concentrations in the Pearl River Delta 2006: a missing OH source in a VOC rich atmosphere, Atmos. Chem. Phys., 12, 1541-1569, 10.5194/acp-12-1541-2012, 2012.

Luecken, D. J., Yarwood, G., and Hutzell, W. T.: Multipollutant modeling of ozone, reactive nitrogen and HAPs across the continental US with CMAQ-CB6, Atmospheric Environment, 201, 62-72, https://doi.org/10.1016/j.atmosenv.2018.11.060, 2019.

Ma, X., Tan, Z., Lu, K., Yang, X., Liu, Y., Li, S., Li, X., Chen, S., Novelli, A., Cho, C., Zeng, L., Wahner, A., and Zhang, Y.: Winter photochemistry in Beijing: Observation and model simulation of OH and HO2 radicals at an urban site, Science of The Total Environment, 685, 85-95, https://doi.org/10.1016/j.scitotenv.2019.05.329, 2019.

Marvin, M. R., Wolfe, G. M., Salawitch, R. J., Canty, T. P., Roberts, S. J., Travis, K. R., Aikin, K. C., de Gouw, J. A., Graus, M., Hanisco, T. F., Holloway, J. S., Hübler, G., Kaiser, J., Keutsch, F. N., Peischl, J., Pollack, I. B., Roberts, J. M., Ryerson, T. B., Veres, P. R., and Warneke, C.: Impact of evolving isoprene mechanisms on simulated formaldehyde: An inter-comparison supported by in situ observations from SENEX, Atmospheric Environment, 164, 325-336, https://doi.org/10.1016/j.atmosenv.2017.05.049, 2017.

Nelson, B. S., Liu, Z. Z., Squires, F. A., Shaw, M., Hopkins, J. R., Hamilton, J. F., Rickard, A. R., Lewis, A. C., Shi, Z. B., and Lee, J. D.: The effect of different climate and air quality policies in China on in situ ozone production in Beijing, ATMOSPHERIC CHEMISTRY AND PHYSICS, 24, 9031-9044, 10.5194/acp-24-9031-2024, 2024.

Park, C., Schade, G. W., and Boedeker, I.: Characteristics of the flux of isoprene and its oxidation products in an urban area, Journal of Geophysical Research: Atmospheres, 116, https://doi.org/10.1029/2011JD015856, 2011.

https://doi.org/10.5194/egusphere-2026-1786
Preprint. Discussion started: 30 April 2026

Sarwar, G., Godowitch, J., Henderson, B. H., Fahey, K., Pouliot, G., Hutzell, W. T., Mathur, R., Kang, D., Goliff, W. S., and Stockwell, W. R.: A comparison of atmospheric composition using the Carbon Bond and Regional Atmospheric Chemistry Mechanisms, ATMOSPHERIC CHEMISTRY AND PHYSICS, 13, 9695-9712, 10.5194/acp-13-9695-2013, 2013.

Scharko, N. K., Berke, A. E., and Raff, J. D.: Release of Nitrous Acid and Nitrogen Dioxide from Nitrate Photolysis in Acidic Aqueous Solutions, Environmental Science & Technology, 48, 11991-12001, 10.1021/es503088x, 2014.

Sha, Q. e., Zhu, M., Huang, H., Wang, Y., Huang, Z., Zhang, X., Tang, M., Lu, M., Chen, C., Shi, B., Chen, Z., Wu, L., Zhong, Z., Li, C., Xu, Y., Yu, F., Jia, G., Liao, S., Cui, X., Liu, J., and Zheng, J.: A newly integrated dataset of volatile organic compounds (VOCs) source profiles and implications for the future development of VOCs profiles in China, Science of The Total Environment, 793, 148348, https://doi.org/10.1016/j.scitotenv.2021.148348, 2021.

She, Y., Li, J., Lyu, X., Guo, H., Qin, M., Xie, X., Gong, K., Ye, F., Mao, J., Huang, L., and Hu, J.: Current status of model predictions of volatile organic compounds and impacts on surface ozone predictions during summer in China, Atmos. Chem. Phys., 24, 219-233, 10.5194/acp-24-219-2024, 2024.

Shu, Z., Liu, Y., Zhao, T., Xia, J., Wang, C., Cao, L., Wang, H., Zhang, L., Zheng, Y., Shen, L., Luo, L., and Li, Y.: Elevated 3D structures of PM_{2.5} and impact of complex terrain-forcing circulations on heavy haze pollution over Sichuan Basin, China, ATMOSPHERIC CHEMISTRY AND PHYSICS, 21, 9253-9268, 10.5194/acp-21-9253-2021, 2021.

Tan, Z., Lu, K., Jiang, M., Su, R., Dong, H., Zeng, L., Xie, S., Tan, Q., and Zhang, Y.: Exploring ozone pollution in Chengdu, southwestern China: A case study from radical chemistry to O3-VOC-NOx sensitivity, Science of The Total Environment, 636, 775-786, https://doi.org/10.1016/j.scitotenv.2018.04.286, 2018.

Tan, Z., Ma, X., Lu, K., Li, X., Zhu, Q., Rohrer, F., Novelli, A., Fuchs, H., Wahner, A., Whalley, L., Heard, D., Brown, S., Zhang, X., and Zhang, Y.: Governing atmospheric oxidation capacity is the key to synergistic air quality and climate gains, One Earth, 9, 101569, https://doi.org/10.1016/j.oneear.2025.101569, 2026.

Tan, Z., Fuchs, H., Lu, K., Hofzumahaus, A., Bohn, B., Broch, S., Dong, H., Gomm, S., Häseler, R., He, L., Holland, F., Li, X., Liu, Y., Lu, S., Rohrer, F., Shao, M., Wang, B., Wang, M., Wu, Y., Zeng, L., Zhang, Y., Wahner, A., and Zhang, Y.: Radical chemistry at a rural site (Wangdu) in the North China Plain: observation and model calculations of OH, HO2 and RO2 radicals, Atmos. Chem. Phys., 17, 663-690, 10.5194/acp-17-663-2017, 2017.

Tang, X. Y., Zhang, Y. H., and Shao, M.: Atmospheric Environmental Chemistry, 2nd edn., Higher Education Press, Beijing2006.

Trinh, H. T., Imanishi, K., Morikawa, T., Hagino, H., and Takenaka, N.: Gaseous nitrous acid (HONO) and nitrogen oxides (NOx) emission from gasoline and diesel vehicles under real-world driving test cycles, JOURNAL OF THE AIR & WASTE MANAGEMENT ASSOCIATION, 67, 412-420, 10.1080/10962247.2016.1240726, 2017.

von Kuhlmann, R., Lawrence, M. G., Pöschl, U., and Crutzen, P. J.: Sensitivities in global scale modeling of isoprene, Atmos. Chem. Phys., 4, 1-17, 10.5194/acp-4-1-2004, 2004.

Wang, H., Li, Y., Liu, Y., Lu, X., Zhang, Y., Fan, Q., Shen, C., Lai, S., Zhou, Y., Zhang, T., and Yue, D.: Underappreciated contributions of biogenic volatile organic compounds from urban green spaces to ozone pollution, Atmos. Chem. Phys., 25, 5233-5250, 10.5194/acp-25-5233-2025, 2025a.

https://doi.org/10.5194/egusphere-2026-1786
Preprint. Discussion started: 30 April 2026

Wang, N., Du, Y., Chen, D., Meng, H., Chen, X., Zhou, L., Shi, G., Zhan, Y., Feng, M., Li, W., Chen, M., Li, Z., and Yang, F.: Spatial disparities of ozone pollution in the Sichuan Basin spurred by extreme, hot weather, Atmos. Chem. Phys., 24, 3029-3042, 10.5194/acp-24-3029-2024, 2024.

Wang, T., Xue, L., Brimblecombe, P., Lam, Y. F., Li, L., and Zhang, L.: Ozone pollution in China: A review of concentrations, meteorological influences, chemical precursors, and effects, Science of The Total Environment, 575, 1582-1596, https://doi.org/10.1016/j.scitotenv.2016.10.081, 2017.

Wang, Y., Li, Q., Wang, Y., Ren, C., Saiz-Lopez, A., Xue, L., and Wang, T.: Increasing soil nitrous acid emissions driven by climate and fertilization change aggravate global ozone pollution, Nature Communications, 16, 2463, 10.1038/s41467-025-57161-6, 2025b.

Wang, Y., Fu, X., Wu, D., Wang, M., Lu, K., Mu, Y., Liu, Z., Zhang, Y., and Wang, T.: Agricultural Fertilization Aggravates Air Pollution by Stimulating Soil Nitrous Acid Emissions at High Soil Moisture, Environmental Science & Technology, 55, 14556-14566, 10.1021/acs.est.1c04134, 2021.

Wang, Y., Yang, X., Wu, K., Mei, H., De Smedt, I., Wang, S., Fan, J., Lyu, S., and He, C.: Long-term trends of ozone and precursors from 2013 to 2020 in a megacity (Chengdu), China: Evidence of changing emissions and chemistry, Atmospheric Research, 278, 106309, https://doi.org/10.1016/j.atmosres.2022.106309, 2022.

Wei, W., Lv, Z. F., Li, Y., Wang, L. T., Cheng, S. Y., and Liu, H.: A WRF-Chem model study of the impact of VOCs emission of a huge petrochemical industrial zone on the summertime ozone in Beijing, China, ATMOSPHERIC ENVIRONMENT, 175, 44-53, 10.1016/j.atmosenv.2017.11.058, 2018.

Xie, Y., Paulot, F., Carter, W. P. L., Nolte, C. G., Luecken, D. J., Hutzell, W. T., Wennberg, P. O., Cohen, R. C., and Pinder, R. W.: Understanding the impact of recent advances in isoprene photooxidation on simulations of regional air quality, Atmos. Chem. Phys., 13, 8439-8455, 10.5194/acp-13-8439-2013, 2013.

Xuan, H. Y., Liu, C., Zhang, P., Chu, B. W., Liang, L. L., Ma, Q. X., and He, H.: A Review of Laboratory Studies on the Heterogeneous Chemistry of NO2: Mechanisms and Uptake Kinetics, JOURNAL OF PHYSICAL CHEMISTRY A, 129, 815-835, 10.1021/acs.jpca.4c07943, 2025.

Xue, L., Gu, R., Wang, T., Wang, X., Saunders, S., Blake, D., Louie, P. K. K., Luk, C. W. Y., Simpson, I., Xu, Z., Wang, Z., Gao, Y., Lee, S., Mellouki, A., and Wang, W.: Oxidative capacity and radical chemistry in the polluted atmosphere of Hong Kong and Pearl River Delta region: analysis of a severe photochemical smog episode, Atmos. Chem. Phys., 16, 9891-9903, 10.5194/acp-16-9891-2016, 2016.

Yan, D., Jin, Z. P., Zhou, Y. T., Li, M. M., Zhang, Z. H., Wang, T. J., Zhuang, B. L., Li, S., and Xie, M.: Anthropogenically and meteorologically modulated summertime ozone trends and their health implications since China's clean air actions, ENVIRONMENTAL POLLUTION, 343, 10.1016/j.envpol.2023.123234, 2024.

Yang, X., Lu, K., Ma, X., Liu, Y., Wang, H., Hu, R., Li, X., Lou, S., Chen, S., Dong, H., Wang, F., Wang, Y., Zhang, G., Li, S., Yang, S., Yang, Y., Kuang, C., Tan, Z., Chen, X., Qiu, P., Zeng, L., Xie, P., and Zhang, Y.: Observations and modeling of OH and HO2 radicals in Chengdu, China in summer 2019, Science of The Total Environment, 772, 144829, https://doi.org/10.1016/j.scitotenv.2020.144829, 2021.

Ye, C., Zhang, N., Gao, H., and Zhou, X.: Photolysis of Particulate Nitrate as a Source of HONO and NOx, Environmental Science & Technology, 51, 6849-6856, 10.1021/acs.est.7b00387, 2017.

Zhang, L., Guo, X., Zhao, T., Gong, S., Xu, X., Li, Y., Luo, L., Gui, K., Wang, H., Zheng, Y., and Yin, X.: A modelling study of the terrain effects on haze pollution in the Sichuan Basin, ATMOSPHERIC ENVIRONMENT, 196, 77-85, 10.1016/j.atmosenv.2018.10.007, 2019.

https://doi.org/10.5194/egusphere-2026-1786
Preprint. Discussion started: 30 April 2026

784 Zhang, S. P., Sarwar, G., Xing, J., Chu, B. W., Xue, C. Y., Sarav, A., Ding, D. A., Zheng, H. T., Mu, Y. J.,
785 Duan, F. K., Ma, T., and He, H.: Improving the representation of HONO chemistry in CMAQ and
786 examining its impact on haze over China, ATMOSPHERIC CHEMISTRY AND PHYSICS, 21, 15809-
787 15826, 10.5194/acp-21-15809-2021, 2021.
788 Zheng, B., Tong, D., Li, M., Liu, F., Hong, C. P., Geng, G. N., Li, H. Y., Li, X., Peng, L. Q., Qi, J., Yan,
789 L., Zhang, Y. X., Zhao, H. Y., Zheng, Y. X., He, K. B., and Zhang, Q.: Trends in China's anthropogenic
790 emissions since 2010 as the consequence of clean air actions, ATMOSPHERIC CHEMISTRY AND
791 PHYSICS, 18, 14095-14111, 10.5194/acp-18-14095-2018, 2018.
792 Zhou, M., Liu, Y., Lu, K., Yu, D., Li, C., Zhai, T., Yang, S., Tan, Z., Ma, X., Li, X., Dong, H., Zeng, L.,
793 Chen, S., Chen, J., Tan, Q., Song, D., Zhang, X., and Zhang, Y.: Ozone production sensitivity analysis
794 for the Chengdu Plain Urban Agglomeration based on a multi-site and two-episode observation, Science
795 of The Total Environment, 950, 175068, https://doi.org/10.1016/j.scitotenv.2024.175068, 2024.
796 Zhou, Z., Tan, Q., Deng, Y., Wu, K., Yang, X., and Zhou, X.: Emission inventory of anthropogenic air
797 pollutant sources and characteristics of VOCs species in Sichuan Province, China, Journal of
798 Atmospheric Chemistry, 76, 21-58, 10.1007/s10874-019-9386-7, 2019.

799